

1  
2  
3  
4  
5  
6  
7  
8  
9  
10  
11  
12  
13  
14  
15  
16  
17  
18  
19  
20  
21

# Deep Meteoric Water Circulation in Earth's Crust

Jennifer C. McIntosh<sup>1,2,\*</sup> and Grant Ferguson<sup>1,2,†</sup>

1. Hydrology and Atmospheric Sciences, University of Arizona, Tucson, AZ 85721 USA
2. Civil, Geological and Environmental Engineering, University of Saskatchewan, Saskatoon, SK CA

*\*corresponding author: [jenmc@email.arizona.edu](mailto:jenmc@email.arizona.edu); 520-626-2282*

*†These authors contributed equally to this work.*

## Key Points

- Maximum circulation depths of meteoric waters vary considerably from <1 to 5km across North America
- The deepest meteoric water circulation occurs in mountainous terrains in western North America
- Topographic gradients and fluid density are important controls on the extent of meteoric water circulation

22 **Abstract**

23

24 Deep meteoric waters comprise a key component of the hydrologic cycle, transferring water,  
25 energy, and life between the earth's surface and deeper crustal environments, yet little is  
26 known about the nature and extent of meteoric water circulation. Using water stable isotopes,  
27 we show that maximum circulation depths of meteoric waters across North America vary  
28 considerably from <1 to 5 km, with the deepest circulation in western North America in areas of  
29 greater topographic relief. Shallower circulation occurs in sedimentary and shield-type  
30 environments with subdued topography. The amount of topographic relief available to drive  
31 regional groundwater flow and flush saline fluids is an important control on the extent of  
32 meteoric water circulation, in addition to permeability. The presence of an active flow system in  
33 the upper few kilometers of the Earth's crust and stagnant brines trapped by negative  
34 buoyancy offers a new framework for understanding deep groundwater systems.

35

36 **Plain Language Summary**

37 Deep circulation of waters, coming from precipitation, connects the Earth's surface with deeper  
38 subsurface environments, transferring water, energy and life critical for key processes, such as  
39 deep mineral weathering and release of nutrients, and geothermal energy systems. Deeper,  
40 more saline groundwater is typically only weakly connected to the rest of the hydrologic cycle.  
41 The penetration depth of precipitation-derived waters and the bottom of the more active  
42 hydrologic cycle is relatively unknown. This study shows the depth of meteoric water circulation  
43 varies considerably across North America as a function of topography and fluid density, in

44 addition to permeability. Study results help constrain locations of deeper meteoric water  
45 penetration and potential hydrologic connections to the earth's surface, which has important  
46 implications for the extent of water resources and transport and long-term storage of  
47 anthropogenic contaminants in the subsurface.

48

#### 49 **Index Terms and Keywords**

50 1829-Groundwater hydrology

51 1041 - Stable isotope geochemistry

52 1832-Groundwater transport

53 1402-Critical Zone

54

55

56 **1. Introduction**

57

58 The extent and controls on deep groundwater circulation are poorly understood, creating  
59 challenges for groundwater resource assessment (Gleeson et al., 2016; Richey et al., 2015),  
60 waste isolation (Cherry et al., 2014; Ferguson, McIntosh, Perrone, et al., 2018), integration of  
61 groundwater into catchment hydrology (Condon et al., 2020; Frisbee et al., 2017) and Critical  
62 Zone science (Küsel et al., 2016), and the distribution and evolution of life in the subsurface  
63 (Lollar et al., 2019; Warr et al., 2018). Permeability exerts an important control on the rate of  
64 groundwater circulation (and groundwater age) and there have been a number of attempts to  
65 assess the variations in permeability with depth (Achtziger-Zupančič et al., 2017; Ingebritsen &  
66 Manning, 1999; Stober & Bucher, 2007). Permeability generally decreases with depth and  
67 residence times increase, however there is no conclusive evidence that groundwater circulation  
68 would cease due to the low permeabilities found at depth (Ingebritsen et al., 2006).

69

70 There have been comparatively few studies that have examined the extent of meteoric  
71 groundwater circulation through compiling geochemical and isotopic evidence. An examination  
72 of the origin of waters in sedimentary basins in North America suggested that topography and  
73 fluid density control the extent of meteoric water circulation rather than permeability  
74 (Ferguson, McIntosh, Grasby, et al., 2018). That study demonstrated that there is insufficient  
75 topography to flush dense brines from the deepest extents of many basins, despite sufficient  
76 permeability. These results were in agreement with  $\delta^2\text{H}$  and  $\delta^{18}\text{O}$  values that fell beneath the  
77 GMWL or a range of other geochemical measures, such as low Cl:Br ratios, that indicated that

78 there was residual paleo-evaporated seawater present in the basin. Here, we build on those  
79 findings to assess the depth to which flushing by meteoric water would be possible in different  
80 geologic terrains at the continental scale using water stable isotopes ( $\delta^2\text{H}$  and  $\delta^{18}\text{O}$ ). We show  
81 that the maximum circulation depth varies considerably over a range of geological  
82 environments across North America and this appears to be associated with the amount of  
83 topographic relief available to overcome the negative buoyancy associated with the density of  
84 saline fluids at depth.

85

## 86 **2. Distribution of Meteoric Waters**

87

88 Meteoric waters typically have  $\delta^2\text{H}$  and  $\delta^{18}\text{O}$  values that fall near the global meteoric water line  
89 (GMWL) (Craig, 1961), and this can be used to delineate groundwaters that originate as  
90 precipitation and have not been significantly modified by water-rock reactions or mixing with  
91 non-meteoric fluids (Ferguson, McIntosh, Grasby, et al., 2018) (Figure 1a). Non-meteoric waters  
92 that deviate from the GMWL can be identified in terms of deuterium excess (D excess) relative  
93 to the GMWL (Dansgaard, 1964):

94

$$95 \quad D \text{ excess} = \delta^2\text{H} - 8 \times \delta^{18}\text{O} \quad [1]$$

96

97 Recognizing that shifts away from the GMWL can occur due to changes in  $\delta^{18}\text{O}$ , this can also be  
98 expressed as oxygen depletion ( $^{18}\text{O}$  depletion) (Kloppmann et al., 2002):

99

100 
$$^{18}\text{O depletion} = \delta^2\text{H}/8 - \delta^{18}\text{O} \quad [2]$$

101

102 At the local scale, meteoric waters plot along local meteoric water lines that have slightly  
103 different slopes and intercepts from the GMWL, depending on local climatic conditions. These  
104 local deviations may over- or underestimate the D excess and  $^{18}\text{O}$  depletion (Kloppmann et al,  
105 2002), and alter the maximum circulation depths approximated in this study.

106

107 Deeper groundwaters that originated as evaporated seawater (e.g., sedimentary basin brines)  
108 typically have  $\delta^2\text{H}$  and  $\delta^{18}\text{O}$  values that plot beneath the GMWL (i.e. negative D excess and  
109 negative  $^{18}\text{O}$  depletion values) (Kharaka & Hanor, 2003). High-temperature (geothermal) waters  
110 plot to the right of the GMWL, enriched in  $^{18}\text{O}$  from high temperature isotope exchange with  
111 minerals; also displaying negative apparent D excess values (Truesdell & Hulston, 1980). Deep  
112 saline waters in cratonic (shield-type) environments often plot to the left of or above the  
113 GMWL due to low temperature water-rock interactions at low water to rock ratios that have  
114 modified either seawater, hydrothermal fluids, and/or meteoric water over long time periods  
115 (Fritz & Frape, 1982; Warr et al., 2020). Fluids that have interacted with  $\text{CO}_2$  can also plot to the  
116 left of the GMWL or to the right (Karolyt  et al., 2017).

117

118 Here we examine  $\delta^2\text{H}$  and  $\delta^{18}\text{O}$  data from water and energy wells and mine inflows to  
119 determine the maximum depth of meteoric water circulation. We supplement these data with  
120 estimated circulation depths for thermal springs where  $\delta^2\text{H}$  and  $\delta^{18}\text{O}$  values of discharged  
121 waters fall along the GMWL.

122

### 123 **3. Methods**

124

#### 125 *3.1. Databases and Mapping*

126

127 The primary databases used to compile  $\delta^2\text{H}$  and  $\delta^{18}\text{O}$  data from wells for this study were the  
128 USGS Produced Waters database (Blondes et al., 2016) and data compiled for the Canadian  
129 Shield (Stotler et al., 2012). These data were supplemented by data from additional studies  
130 (Clark et al., 1998; Mariner & Janik, 1995; McIntosh et al., 2002, 2008, 2010; Osburn et al.,  
131 2019; Zhang et al., 2009). These datasets were culled to consider only those samples that  
132 provided a well location and depth. Additional data from the USGS NAWQA dataset (USGS,  
133 2020) were also used to understand the distribution of meteoric water with depth in this study,  
134 but were not considered during mapping because of the shallow depth of most water supply  
135 wells and associated groundwater quality monitoring.

136

#### 137 *3.2. Estimating Meteoric Water Circulation Depths*

138

139 Meteoric waters are typically defined as waters with  $\delta^2\text{H}$  and  $\delta^{18}\text{O}$  values falling near the  
140 GMWL. However, meteoric waters vary in their distance from the meteoric water line due to a  
141 range of processes, such as partial evaporation and convective air mass mixing that create local  
142 meteoric water lines (Jasechko, 2019). Tolerances for where meteoric waters fall around the  
143 GMWL are not typically defined quantitatively. Here, we consider waters with D excess values

144 falling between -10 and 30‰ (20‰ variability in  $\delta^2\text{H}$  or 2.5‰ variability in  $\delta^{18}\text{O}$  around the  
145 GMWL) as meteoric waters.

146

147 To supplement  $\delta^2\text{H}$  and  $\delta^{18}\text{O}$  data from wells, we used studies that have estimated maximum  
148 temperatures from aqueous geothermometry on samples collected from thermal springs  
149 discharging meteoric water (Davisson et al., 1994; Frisbee et al., 2017; Grasby et al., 2016;  
150 Grasby & Hutcheon, 2001; Mayo & Loucks, 1995; Pepin et al., 2015). Those studies used local  
151 geothermal gradients to estimate the circulation depth required to obtain those maximum  
152 temperatures.

153

154 The maximum depth of circulation was estimated by determining the maximum depth of water  
155 samples with a D excess value falling between -10 and 30‰ or estimated circulation depth of a  
156 thermal spring with a meteoric water isotope signature based on a 2 degree by 2 degree grid  
157 across North America. Over much of North America, especially outside of oil and gas producing  
158 regions, the availability of deep samples is limited, and our mapped results are likely to  
159 underestimate the depth to which meteoric water is present. In addition, the approach used  
160 here underestimates meteoric water circulation depth by not considering deeper meteoric  
161 waters that have been isotopically-altered through low or high temperature water-rock  
162 reactions, or through isotopic exchange with  $\text{CO}_2$ . Where no samples deeper than 500 m were  
163 available, the grid spaces were left blank during mapping.

164

165 *3.3. Assessment of Topography and Driving Force Ratio*

166

167 We assess the possibility that the distribution of meteoric waters is controlled by the amount of  
168 topography available to drive regional groundwater flow and the negative buoyancy of dense,  
169 saline fluids at depth. Darcy's law for variable density groundwater flow can be written as:

$$170 \quad q = \frac{-\mu}{\mu_o} K \left( \nabla h_o - \frac{\Delta\rho}{\rho_o} \nabla z \right) \quad [3]$$

171 Where  $q$  is specific discharge,  $\mu$  is viscosity,  $\mu_o$  is a reference viscosity,  $h_o$  is hydraulic head at a  
172 given reference density,  $\rho$  is density,  $\rho_o$  is reference density (commonly assumed to be 1,000  
173 kg/m<sup>3</sup>) and  $z$  is elevation head (Figure 2).

174 And

$$175 \quad h_o = \frac{p}{\rho_o g} + z \quad [4]$$

176 Where  $p$  is fluid pressure and  $g$  is acceleration due to gravity. The force driving groundwater  
177 flow, which determines the magnitude and direction of the hydraulic gradient, can be described  
178 as (Bachu, 1995):

$$179 \quad F = -\frac{g\rho_o}{\rho} \left( \nabla h_o + \frac{\nabla\rho}{\rho_o} \nabla E \right) = F_p + F_b \quad [5]$$

180 Where  $\nabla h_o$  is the hydraulic gradient based on a reference density and  $\nabla E$  is the average  
181 structural gradient of the groundwater flow system (i.e. the slope that the water must travel  
182 along to exit the groundwater system). The relative importance of  $F_p$ , which is the force  
183 associated with topographic differences, and  $F_b$ , which is the force of negative buoyancy, is  
184 described by the driving force ratio (DFR), which is defined as follows (Bachu, 1995):

185

$$186 \quad DFR = \left( \frac{\Delta\rho}{\rho_o} \frac{|\nabla E|}{|\nabla h_o|} \right) \quad [6]$$

187

188 This approach was originally intended to assess errors arising from using potentiometric maps  
189 based on reference densities, but has been extended to examine where dense brines would be  
190 trapped by negative buoyancy in sedimentary basins (Ferguson, McIntosh, Grasby, et al., 2018).

191 In this case, the condition necessary for waters to stagnate can be described as:

192

$$193 \quad \nabla h_o = \frac{\Delta\rho}{\rho_o} \nabla E \quad [7]$$

194

195 For systems where the water table closely follows the topography and the highest hydraulic  
196 head in the flow system overlies the deepest point of the flow system, [3] can be approximated  
197 as:

198

$$199 \quad \Delta h_{max} = \frac{\rho - \rho_o}{\rho_o} z_{max} \quad [8]$$

200

201 Where  $\Delta h_{max}$  is the maximum hydraulic head and  $z_{max}$  is the maximum circulation depth. Where  
202  $h_o$  is insufficient to overcome the density contrast, dense waters below  $z_{max}$  are isolated from  
203 the overlying topographically-driven flow system and will not discharge to surface water  
204 bodies. The case where the deepest part of the flow system coincides with the maximum  
205 ground surface elevation will underestimate *DFR* in most cases. If the deepest part of the flow  
206 system coincides with its horizontal midpoint,  $|\nabla E|$  would increase by a factor of two and [5]  
207 would overestimate circulation depth by the same factor.

208

209 Here, we use topographic drops as a proxy for the maximum hydraulic head change. This will  
210 tend to overestimate hydraulic gradients, especially in areas with higher permeability, lower  
211 recharge rates or higher topography (Gleeson et al., 2011), resulting in overestimation of the  
212 maximum circulation depth. Maximum topographic drops were calculated from the USGS  
213 GTOPO30 digital elevation model (USGS, 1997) on a 2 degree x 2 degree grid across North  
214 America using QGIS. We chose a gridded approach because there are many areas of North  
215 America where there are no obvious boundaries for deep groundwater flow systems.  
216 Permeability contrasts associated with geological contacts have been used to constrain these in  
217 some studies (Ferguson, McIntosh, Grasby, et al., 2018; Condon et al., 2020). This approach is  
218 ill-suited for the current problem because it assumes that meteoric water will not circulate  
219 through lower permeability rocks. Watershed-based approaches are also problematic because  
220 deep groundwater flow often transfers water between watersheds (Fan, 2019). These  
221 topographic drops are then compared to the sample depths in each grid block to calculate the  
222 topographic drop to depth ratio.

223

#### 224 **4. Maximum Circulation Depth**

225

226 The maximum circulation depth of meteoric waters in North America ranges from less than 1  
227 km in eastern North America to approximately 5 km in the west (Figure 3). Deeper circulation  
228 depths occur in areas of greater topographic relief and the greatest circulation depths are  
229 associated with thermal springs. The shallowest circulation depths are associated with oil/gas  
230 produced waters in sedimentary basins and mines in crystalline bedrock.

231

232 Lithology does not appear to exert a strong control on circulation depth. The circulation depths  
233 in the Canadian Shield are similar to many sedimentary basins in midcontinent North America,  
234 despite the large differences in permeability (Figure 1b). The extent of meteoric water  
235 circulation in the Canadian Shield roughly coincides with the depth where bulk permeability  
236 approaches the matrix permeability at ~1 km (Achtziger-Zupančič et al., 2017). While  
237 permeability and meteoric water circulation appear to coincide in the Canadian Shield,  
238 examination of other environments suggests that permeability might not be the only  
239 controlling factor.

240

241 In sedimentary basins, decreases in permeability with depth do not explain the extent of  
242 meteoric water circulation. Over much of central North America, circulation depths are less  
243 than 2 km. Relatively high permeability ( $>10^{-16} \text{ m}^2$ ) sandstone and carbonate aquifers are  
244 present at the bottom of many sedimentary basins ( $> 2 \text{ km}$  depth) (Figure 1b). Yet these basal  
245 aquifer systems often contain non-meteoric waters, derived from paleo-evaporated seawater  
246 (Bein & Dutton, 1993; Ferguson et al., 2007; Stueber & Walter, 1991). Conventional oil and gas  
247 production and saltwater disposal are common in these deep strata (Ferguson, 2015; Scanlon  
248 et al., 2019; Zhang et al., 2016), indicating that appreciable groundwater flow rates are possible  
249 where hydraulic gradients are sufficiently high. In some cases, such as the lower Paleozoic  
250 aquifers of the Williston Basin, these systems appear to be hydraulically continuous between  
251 known recharge and discharge areas (Bachu and Hitchon, 1996; Grasby et al., 2000; Ferguson et

252 al., 2007). We hypothesize an additional mechanism for trapping saline fluids at depth in  
253 sedimentary and crystalline environments - due to negative buoyancy.

254

255 The deepest circulation of meteoric groundwater is found in thermal springs in mountainous  
256 areas of western North America. The median circulation depth of the 38 springs compiled here  
257 was 2.6 km and this approach is thought to underestimate circulation depth due to  
258 geochemical re-equilibration of waters as they interact with the rock mass as they rise toward  
259 the discharge area, and due to mixing of waters from different depths (Ferguson et al., 2009).

260 The results presented here are similar to those found in the Alps (Diamond et al., 2018;  
261 Luijendijk et al., 2020). Very little is known about the permeability distribution of these systems  
262 from direct measurements, but numerical modelling indicates that country rock values on the  
263 order of  $10^{-16} \text{ m}^2$  are required to supply a sufficient amount of water to a fault to support the  
264 formation of thermal springs (Forster & Smith, 1989).

265

266 The link between topography and circulation depth indicates that the forces driving circulation  
267 may exert a substantial control on how deep meteoric water penetrates into the Earth's crust.  
268 Deep groundwaters that do not fall on the GMWL typically have salinities that are several times  
269 that of seawater (Fritz & Frape, 1982; Kharaka & Hanor, 2003). These highly saline waters  
270 appear to be ubiquitous at depth in both sedimentary environments (Kharaka & Hanor, 2003)  
271 and in crystalline bedrock (Stotler et al., 2012; Warr et al., 2018) and are also thought to be  
272 present in the lower crust (Manning, 2018). Due to their high salinities (TDS~300 g/L), these  
273 waters have densities that approach  $1,200 \text{ kg/m}^3$  (Adams & Bachu, 2002). For regional

274 groundwater flow systems where the water table coincides with the ground surface, the  
275 topographic drop to depth ratio must exceed 0.2 for a 1,200 kg/m<sup>3</sup> density brine to allow for it  
276 to be flushed by meteoric water (Equation 8). Actual topographic drop to depth ratios required  
277 for flushing would be greater than 0.2, as regional hydraulic gradients are less than topographic  
278 gradients.

279

280 Meteoric waters with D excess values between -10 and 30‰ and <sup>18</sup>O depletion values from -  
281 1.25 to 3.75‰, corresponding to the GMWL, tend to have large topographic drops relative to  
282 their depths. Where topographic drop to depth ratios of less than 0.2 and trapping due to  
283 negative buoyancy is expected, D excess values tend to be less than -10‰ and <sup>18</sup>O depletion  
284 values tend to be less than -1.25‰ (Figure 4). In some cases, meteoric waters are found at  
285 topographic drop to depth ratios of less than 0.2, in locations where increased hydraulic  
286 gradients from Pleistocene ice sheets (McIntosh et al., 2002; McIntosh et al., 2011) or due to  
287 sea-level low stands in coastal aquifers (Person et al., 2003; Cohen et al., 2010; Post et al., 2013)  
288 enhanced meteoric circulation and flushing of basinal brines or seawater, respectively.

289

290 The most negative D excess and <sup>18</sup>O depletion values (i.e., most saline basin brines) are  
291 associated with topographic drop to depth ratios less than ~1, although a variety of D excess  
292 and <sup>18</sup>O depletion values are found at these ratios. <sup>18</sup>O depletion and apparent D excess values  
293 exceeding +3.75‰ and +30‰, respectively (i.e., shield-type brines) tend to be associated with  
294 topographic drop to depth ratios of ~1.

295

296 Many of the samples with D excess and  $^{18}\text{O}$  depletion values outside of the range expected  
297 from meteoric waters have topographic drop to depth ratios greater than the critical value (0.2)  
298 or higher than is required to displace a brine with a density of  $1,200 \text{ kg/m}^3$  (Figure 4). Many of  
299 these samples likely have a component of meteoric water that is actively circulating or are  
300 residual brines that are still in the process of being flushed by regional groundwater flow, which  
301 may take millions of years or more due to the presence of low permeability units. Ingebritsen  
302 and Manning (1999) estimate that crustal permeability is typically greater than  $10^{-16} \text{ m}^{12}$  in the  
303 upper 5,000 m, which would allow for movement of fluids over distances of kilometers over  
304 periods of a few million years. In extreme cases, such as permeabilities below  $10^{-20} \text{ m}^2$  known to  
305 exist in intact crystalline rock (Achtziger-Zupančič et al., 2017), evaporites (Bredehoeft, 1988),  
306 and shale (Neuzil, 1986), advective transport of only a few m in 100s of millions of years is  
307 possible, preventing any meaningful flushing by meteoric waters. For example, the most  
308 ancient shield-type brines may be trapped in isolated fractures that are disconnected from  
309 active circulation systems due to extremely low permeabilities (Warr et al., 2018).

310 Other non-meteoric water samples that have a topographic drop to depth ratio greater  
311 than the critical value (0.2) could be trapped by negative buoyancy due to the overestimation  
312 of the hydraulic gradient by using topography as a proxy (e.g., in areas with deep water tables  
313 that are a subdued reflection of surface topography) or by underestimating the structural  
314 gradient (e.g., instances where the highest hydraulic head values does not overlie the maximum  
315 circulation depth) (Ferguson, McIntosh, Grasby, et al., 2018).

316

## 317 **5. Conclusions - Rethinking the Extent of the Deep Hydrological Cycle**

318

319 Many previous studies have assumed that groundwater resources extended to 1 or 2 km  
320 globally (Gleeson et al., 2016; Nace, 1969; Richey et al., 2015). The remarkable spatial variability  
321 of circulation depth suggests that previous estimates of the volume (Gleeson et al., 2016; Nace,  
322 1969; Richey et al., 2015) and residence times of groundwater at global scales (Befus et al.,  
323 2017) are less certain, depending on topographic gradients, permeability structure and salinity  
324 distribution. Taking into account this variability and fluid drivers provides an opportunity to  
325 refine global estimates of groundwater volumes and circulation depths.

326

327 Topography and variations of fluid density with depth exert a strong control on the extent of  
328 the meteoric water circulation in the crust, in addition to permeability decreases, which have  
329 received more attention to-date as a primary constraint on the circulation of groundwater at  
330 depth (Achtziger-Zupančič et al., 2017; Ingebriten & Manning, 1999; Ingebriten & Gleeson,  
331 2017; Ranjram et al., 2015; Stober & Bucher, 2007). Global assessments of bulk permeability  
332 have suggested that groundwater flow is possible over most of the brittle crust, which extends  
333 to a depth of ~10 km (Ingebriten & Manning, 1999). Our results indicate that circulation of  
334 meteoric water outside of orogenic belts is largely restricted to the upper 1 to 2 km, regardless  
335 of permeability and is influenced by topography and negative buoyancy. The inability of  
336 meteoric water to circulate to depths exceeding more than ~1 to 2 km over large areas of  
337 continents is consistent with observations of very old, saline waters at these depths in both  
338 cratons (Holland et al., 2013; Lippmann et al., 2003; Warr et al., 2018) and sedimentary basins  
339 (Castro et al., 1998; Zhou & Ballentine, 2006). It is also consistent with penetration depths of

340 meteoric waters that have recently been in contact with the atmosphere based on the presence  
341 of tritium (Gleeson et al., 2016) and radiocarbon (Jasechko et al., 2017).

342

343 These results showing the importance of topographic gradients and fluid density elicit a change  
344 in how we characterize hydrogeologic systems. We have few tools other than sampling deep  
345 wells, boreholes or mines to characterize groundwater salinity and residence times at depth. In  
346 particular, deep wells are uncommon in mountainous regions (Markovich et al., 2019) – areas  
347 with the deepest meteoric water circulation – and beyond ~1 km in crystalline shield-type  
348 environments. The need for geophysical or other techniques to address the extent of meteoric  
349 groundwater in the Earth’s crust represents a major challenge for the geosciences.

350

### 351 **Acknowledgements**

352 This project was supported by a Global Water Futures grant to Ferguson and McIntosh and an  
353 NSERC Discovery Grant to Ferguson. McIntosh also acknowledges funding from the W.M. Keck  
354 Foundation and CIFAR Earth4D: Subsurface Science and Exploration Program. Thank you to the  
355 reviewers for providing helpful comments that improved the manuscript. Data is available from  
356 Blondes et al. (2016), Clark et al. (1998), Davisson et al. (1994), Frisbee et al. (2017), Grasby et  
357 al. (2016), Grasby & Hutcheon (2001), Mayo & Loucks (1995), Mariner & Janik (1995), McIntosh  
358 et al. (2002; 2008; 2010), Osburn et al. (2019), Pepin et al. (2015), Stotler et al. (2012), USGS  
359 (2020), and Zhang et al. (2009).

360

361

362 **References**

363

364

365 Achtziger-Zupančič, P., Loew, S., & Mariethoz, G. (2017). A new global database to improve

366 predictions of permeability distribution in crystalline rocks at site scale. *Journal of*

367 *Geophysical Research: Solid Earth*, 122(5), 3513–3539.

368 Adams, J., & Bachu, S. (2002). Equations of state for basin geofluids: algorithm review and

369 intercomparison for brines. *Geofluids*, 2(4), 257–271.

370 Bachu, S. (1995). Flow of variable-density formation water in deep sloping aquifers: review of

371 methods of representation with case studies. *Journal of Hydrology*, 164(1), 19–38.

372 Bachu, S., & Hitchon, B. (1996). Regional-scale flow of formation waters in the Williston Basin.

373 *AAPG Bulletin*, 80(2), 248-264.

374 Befus, K. M., Jasechko, S., Luijendijk, E., Gleeson, T., & Cardenas, M. B. (2017). The rapid yet

375 uneven turnover of Earth's groundwater. *Geophysical Research Letters*, 44(11), 5511-

376 5520.

377 Bein, A., & Dutton, A. R. (1993). Origin, distribution, and movement of brine in the Permian

378 Basin (USA): A model for displacement of connate brine. *Geological Society of America*

379 *Bulletin*, 105(6), 695–707.

380 Blondes, M. S., Gans, K. D., Thordsen, J. J., Reidy, M. E., Thomas, B., Engle, M. A., et al. (2016).

381 US Geological Survey National Produced Waters Geochemical Database v2. 3

382 (PROVISIONAL). *United States Geological Survey*.

383 Bredehoeft, J. D. (1988). Will salt repositories be dry? *EOS, Transactions American Geophysical*

384 *Union*, 69(9), 121-131.

385 Castro, M. C., Jambon, A., De Marsily, G., & Schlosser, P. (1998). Noble gases as natural tracers  
386 of water circulation in the Paris Basin: 1. Measurements and discussion of their origin  
387 and mechanisms of vertical transport in the basin. *Water Resources Research*, 34(10),  
388 2443–2466.

389 Cherry, J. A., Alley, W. M., & Parker, B. L. (2014). Geologic Disposal of Spent Nuclear Fuel. *The*  
390 *Bridge on Emerging Issues in Earth Resources Engineering*, 44(1), 51–59.

391 Clark, J. F., Davisson, M. L., Hudson, G. B., & Macfarlane, P. A. (1998). Noble gases, stable  
392 isotopes, and radiocarbon as tracers of flow in the Dakota aquifer, Colorado and Kansas.  
393 *Journal of Hydrology*, 211(1–4), 151–167.

394 Cohen, D., Person, M., Wang, P., Gable, C. W., Hutchinson, D., Marksamer, A., Dugan, B., Kooi,  
395 H., Groen, K., Lizarralde, D. & Evans, R. L. (2010). Origin and extent of fresh paleowaters  
396 on the Atlantic continental shelf, USA. *Groundwater*, 48(1), 143-158.

397 Condon, L. E., Markovich, K. H., Kelleher, C. A., McDonnell, J. J., Ferguson, G., & McIntosh, J. C.  
398 (2020). Where is the bottom of a watershed? *Water Resources Research*, 56(3).

399 Craig, H. (1961). Isotopic variations in meteoric waters. *Science*, 133(3465), 1702–1703.

400 Dansgaard, W. (1964). Stable isotopes in precipitation. *Tellus*, 16(4), 436–468.

401 Davisson, M. L., Presser, T. S., & Criss, R. E. (1994). Geochemistry of tectonically expelled fluids  
402 from the northern Coast ranges, Rumsey Hills, California, USA. *Geochimica et*  
403 *Cosmochimica Acta*, 58(7), 1687–1699.

404 Diamond, L. W., Wanner, C., & Waber, H. N. (2018). Penetration depth of meteoric water in  
405 orogenic geothermal systems. *Geology*, 46(12), 1063–1066.

406 Fan, Y. (2019). Are catchments leaky? *Wiley Interdisciplinary Reviews: Water*, 6(6), e1386.

407 Ferguson, G. (2015). Deep Injection of Waste Water in the Western Canada Sedimentary Basin.  
408 *Groundwater*, 53(2), 187–194. <https://doi.org/10.1111/gwat.12198>

409 Ferguson, G., Betcher, R. N., & Grasby, S. E. (2007). Hydrogeology of the Winnipeg Formation in  
410 Manitoba, Canada. *Hydrogeology Journal*, 15(3), 573–587.  
411 <https://doi.org/10.1007/s10040-006-0130-4>

412 Ferguson, G., Grasby, S. E., & Hindle, S. R. (2009). What do aqueous geothermometers really tell  
413 us? *Geofluids*, 9(1), 39–48. <https://doi.org/10.1111/j.1468-8123.2008.00237.x>

414 Ferguson, G., McIntosh, J. C., Perrone, D., & Jasechko, S. (2018). Competition for shrinking  
415 window of low salinity groundwater. *Environmental Research Letters*, 13, 114013.

416 Ferguson, G., McIntosh, J. C., Grasby, S. E., Hendry, M. J., Jasechko, S., Lindsay, M. B. J., &  
417 Luijendijk, E. (2018). The Persistence of Brines in Sedimentary Basins. *Geophysical*  
418 *Research Letters*, 45(10), 4851–4858.

419 Forster, C., & Smith, L. (1989). The influence of groundwater flow on thermal regimes in  
420 mountainous terrain: A model study. *Journal of Geophysical Research: Solid Earth*,  
421 94(B7), 9439–9451. <https://doi.org/10.1029/JB094iB07p09439>

422 Frisbee, M. D., Tolley, D. G., & Wilson, J. L. (2017). Field estimates of groundwater circulation  
423 depths in two mountainous watersheds in the western US and the effect of deep  
424 circulation on solute concentrations in streamflow. *Water Resources Research*, 53(4),  
425 2693–2715.

426 Fritz, P., & Frape, S. t. (1982). Saline groundwaters in the Canadian Shield—a first overview.  
427 *Chemical Geology*, 36(1), 179–190.

428 Gleeson, T., Marklund, L., Smith, L., & Manning, A. H. (2011). Classifying the water table at  
429 regional to continental scales. *Geophysical Research Letters*, 38(5).

430 Gleeson, T., Befus, K. M., Jasechko, S., Luijendijk, E., & Cardenas, M. B. (2016). The global  
431 volume and distribution of modern groundwater. *Nature Geoscience*, 9(2), 161–167.

432 Grasby, S. E., & Hutcheon, I. (2001). Controls on the distribution of thermal springs in the  
433 southern Canadian Cordillera. *Canadian Journal of Earth Sciences*, 38(3), 427–440.

434 Grasby, S. E., Ferguson, G., Brady, A., Sharp, C., Dunfield, P., & McMechan, M. (2016). Deep  
435 groundwater circulation and associated methane leakage in the northern Canadian  
436 Rocky Mountains. *Applied Geochemistry*, 68, 10–18.

437 Grasby, S., Osadetz, K., Betcher, R., & Render, F. (2000). Reversal of the regional-scale flow  
438 system of the Williston basin in response to Pleistocene glaciation. *Geology*, 28(7), 635–  
439 638.

440 Holland, G., Lollar, B. S., Li, L., Lacrampe-Couloume, G., Slater, G., & Ballentine, C. (2013). Deep  
441 fracture fluids isolated in the crust since the Precambrian era. *Nature*, 497(7449), 357.

442 Ingebritsen, S. E., & Gleeson, T. (2017). Crustal permeability. *Hydrogeology Journal*, 25(8),  
443 2221–2224.

444 Ingebritsen, S. E., & Manning, C. E. (1999). Geological implications of a permeability-depth  
445 curve for the continental crust. *Geology*, 27(12), 1107–1110.

446 Ingebritsen, S. E., Sanford, W. E., & Neuzil, C. (2006). *Groundwater in Geologic Processes*.  
447 Cambridge University Press.

448 Jasechko, S. (2019). Global isotope hydrogeology—Review. *Reviews of Geophysics*, 57(3), 835–  
449 965.

450 Jasechko, S., Perrone, D., Befus, K. M., Cardenas, M. B., Ferguson, G., Gleeson, T., et al. (2017).  
451 Global aquifers dominated by fossil groundwaters but wells vulnerable to modern  
452 contamination. *Nature Geoscience*, *10*(6), 425–429.

453 Karolytè, R., Serno, S., Johnson, G., & Gilfillan, S. M. (2017). The influence of oxygen isotope  
454 exchange between CO<sub>2</sub> and H<sub>2</sub>O in natural CO<sub>2</sub>-rich spring waters: Implications for  
455 geothermometry. *Applied Geochemistry*, *84*, 173–186.

456 Kharaka, Y. K., & Hanor, J. S. (2003). Deep fluids in the continents: I. Sedimentary basins.  
457 *Treatise on Geochemistry*, *5*, 605.

458 Kloppmann, W., Girard, J.-P., & Négre, P. (2002). Exotic stable isotope compositions of saline  
459 waters and brines from the crystalline basement. *Chemical Geology*, *184*(1–2), 49–70.

460 Küsel, K., Totsche, K. U., Trumbore, S. E., Lehmann, R., Steinhäuser, C., & Herrmann, M. (2016).  
461 How deep can surface signals be traced in the critical zone? Merging biodiversity with  
462 biogeochemistry research in a central German Muschelkalk landscape. *Frontiers in Earth  
463 Science*, *4*, 32.

464 Lippmann, J., Stute, M., Torgersen, T., Moser, D. P., Hall, J. A., Lin, L., et al. (2003). Dating ultra-  
465 deep mine waters with noble gases and <sup>36</sup>Cl, Witwatersrand Basin, South Africa.  
466 *Geochimica et Cosmochimica Acta*, *67*(23), 4597–4619.

467 Lollar, G. S., Warr, O., Telling, J., Osburn, M. R., & Lollar, B. S. (2019). ‘Follow the Water’:  
468 Hydrogeochemical Constraints on Microbial Investigations 2.4 km Below Surface at the  
469 Kidd Creek Deep Fluid and Deep Life Observatory. *Geomicrobiology Journal*, 1–14.

470 Luijendijk, E., Winter, T., Köhler, S., Ferguson, G., von Hagke, C. & Scibek, J. (2020) Using  
471 thermal springs to quantify deep groundwater flow and its thermal footprint in the Alps

472 and a comparison with North American orogens. *Geophysical Research Letters*,  
473 doi:10.1029/2020GL090134.

474 Manning, C. E. (2018). Fluids of the lower crust: deep is different. *Annual Review of Earth and*  
475 *Planetary Sciences*, 46, 67–97.

476 Mariner, R. H., & Janik, C. J. (1995). *Geochemical data and conceptual model for the Steamboat*  
477 *Hills geothermal system, Washoe County, Nevada*. Geothermal Resources Council, Davis,  
478 CA (United States).

479 Markovich, K. H., Manning, A. H., Condon, L. E., & McIntosh, J. C. (2019). Mountain-Block  
480 Recharge: A Review of Current Understanding. *Water Resources Research*, 55(11), 8278–  
481 8304.

482 Mayo, A. L., & Loucks, M. D. (1995). Solute and isotopic geochemistry and ground water flow in  
483 the central Wasatch Range, Utah. *Journal of Hydrology*, 172(1–4), 31–59.

484 McIntosh, J. C., Walter, L., & Martini, A. (2002). Pleistocene recharge to midcontinent basins:  
485 effects on salinity structure and microbial gas generation. *Geochimica et Cosmochimica*  
486 *Acta*, 66(10), 1681–1700.

487 McIntosh, J. C., Martini, A., Petsch, S., Huang, R., & Nüsslein, K. (2008). Biogeochemistry of the  
488 Forest City Basin coalbed methane play. *International Journal of Coal Geology*, 76(1–2),  
489 111–118.

490 McIntosh, J. C., Warwick, P. D., Martini, A. M., & Osborn, S. G. (2010). Coupled hydrology and  
491 biogeochemistry of Paleocene–Eocene coal beds, northern Gulf of Mexico. *Bulletin*,  
492 122(7–8), 1248–1264.

493 McIntosh, J. C., Garven, G. & Hanor, J. S. (2011). Impacts of Pleistocene glaciation on large-scale  
494 groundwater flow and salinity in the Michigan Basin. *Geofluids*, 11(1), 18-33.

495 Medina, C. R., Rupp, J. A., & Barnes, D. A. (2011). Effects of reduction in porosity and  
496 permeability with depth on storage capacity and injectivity in deep saline aquifers: A  
497 case study from the Mount Simon Sandstone aquifer. *International Journal of*  
498 *Greenhouse Gas Control*, 5(1), 146–156.

499 Nace, R. L. (1969). World water inventory and control. In R. J. Chorley (Ed.), *Water, Earth, and*  
500 *Man* (pp. 31–42). London, U.K.: Methuen.

501 Neuzil, C. E. (1986). Groundwater flow in low-permeability environments. *Water Resources*  
502 *Research*, 22(8), 1163-1195.

503 Osburn, M. R., Kruger, B., Masterson, A., Casar, C., & Amend, J. (2019). Establishment of the  
504 Deep Mine Microbial Observatory (DeMMO), South Dakota, USA, a geochemically stable  
505 portal into the deep subsurface. *Frontiers in Earth Science*, 7, 196.

506 Pepin, J., Person, M., Phillips, F., Kelley, S., Timmons, S., Owens, L., et al. (2015). Deep fluid  
507 circulation within crystalline basement rocks and the role of hydrologic windows in the  
508 formation of the Truth or Consequences, New Mexico low-temperature geothermal  
509 system. *Geofluids*, 15(1–2), 139–160.

510 Person, M., Dugan, B., Swenson, J.B., Urbano, L., Stott, C., Taylor, J., & Willet, M. (2003).  
511 Pleistocene hydrogeology of the Atlantic continental shelf, New England. *Geological*  
512 *Society of America Bulletin*, 115(11), 1324-1343.

513 Phillips, D. (2019). *Reservoir Characterization and Modeling of Potash Mine Injection Wells in*  
514 *Saskatchewan*. University of Saskatchewan, Saskatoon, SK.

516 Post, V. E., Groen, J., Kooi, H., Person, M., Ge, S., & Edmunds, W. M. (2013). Offshore fresh  
517 groundwater reserves as a global phenomenon. *Nature*, *504*(7478), 71-78.

518 Ranjram, M., Gleeson, T., & Luijendijk, E. (2015). Is the permeability of the crystalline rock in the  
519 shallow crust related to depth, lithology or tectonic setting? *Geofluids*, *15*(1-2), 106-199.

520 Richey, A. S., Thomas, B. F., Lo, M., Famiglietti, J. S., Swenson, S., & Rodell, M. (2015).  
521 Uncertainty in global groundwater storage estimates in a Total Groundwater Stress  
522 framework. *Water Resources Research*, *51*(7), 5198–5216.  
523 <https://doi.org/10.1002/2015WR017351>

524 Scanlon, B. R., Weingarten, M. B., Murray, K. E., & Reedy, R. C. (2019). Managing Basin-Scale  
525 Fluid Budgets to Reduce Injection-Induced Seismicity from the Recent U.S. Shale Oil  
526 Revolution. *Seismological Research Letters*, *90*(1), 171–182.  
527 <https://doi.org/10.1785/0220180223>

528 Stober, I., & Bucher, K. (2007). Hydraulic properties of the crystalline basement. *Hydrogeology*  
529 *Journal*, *15*(2), 213–224.

530 Stotler, R., Frape, S., Ruskeeniemi, T., Pitkänen, P., & Blowes, D. (2012). The interglacial–glacial  
531 cycle and geochemical evolution of Canadian and Fennoscandian Shield groundwaters.  
532 *Geochimica et Cosmochimica Acta*, *76*, 45–67.

533 Stueber, A. M., & Walter, L. M. (1991). Origin and chemical evolution of formation waters from  
534 Silurian-Devonian strata in the Illinois Basin, USA. *Geochimica et Cosmochimica Acta*,  
535 *55*(1), 309–325.

536 Truesdell, A. H., & Hulston, J. R. (1980). Isotopic evidence on environments of geothermal  
537 systems. In Fritz, P., Fontes, J.Ch. (Eds.) *Handbook of environmental isotope*  
538 *geochemistry. Vol. 1*, Elsevier, Amsterdam, pp. 179-226.

539 USGS (1997). USGS 30 ARC-second Global Elevation Data, GTOPO30. Boulder, CO: Research  
540 Data Archive at the National Center for Atmospheric Research, Computational and  
541 Information Systems Laboratory. <https://doi.org/10.5065/A1Z4-EE71>

542 USGS (2020). National Water-Quality Assessment (NAWQA). Retrieved from  
543 [https://www.usgs.gov/mission-areas/water-resources/science/national-water-quality-](https://www.usgs.gov/mission-areas/water-resources/science/national-water-quality-assessment-nawqa)  
544 [assessment-nawqa](https://www.usgs.gov/mission-areas/water-resources/science/national-water-quality-assessment-nawqa)

545 Warr, O., Sherwood Lollar, B., Fellowes, J., Sutcliffe, C. N., McDermott, J. M., Holland, G., et al.  
546 (2018). Tracing ancient hydrogeological fracture network age and compartmentalisation  
547 using noble gases. *Geochimica et Cosmochimica Acta*, 222, 340–362.

548 Warr, O., Giunta, T., Onstott, T., Kieft, T., Harris, R., Nisson, D., & Sherwood Lollar, B. (2020).  
549 Subsurface 18O Exchange at Low Temperatures: The (GMWL) Plot Thickens. Presented  
550 at the Goldschmidt Virtual 2020, The Geochemical Society.

551 Zhang, Y., Edel, S. S., Pepin, J., Person, M., Broadhead, R., Ortiz, J. P., et al. (2016). Exploring the  
552 potential linkages between oil-field brine reinjection, crystalline basement permeability,  
553 and triggered seismicity for the Dagger Draw Oil field, southeastern New Mexico, USA,  
554 using hydrologic modeling. *Geofluids*, 16(5), 971–987.

555 Zhang, Y., Gable, C. W., Zvoloski, G. A., & Walter, L. M. (2009). Hydrogeochemistry and gas  
556 compositions of the Uinta Basin: A regional-scale overview. *AAPG Bulletin*, 93(8), 1087–  
557 1118.

558 Zhou, Z., & Ballentine, C. J. (2006).  $^4\text{He}$  dating of groundwater associated with hydrocarbon  
559 reservoirs. *Chemical Geology*, 226(3–4), 309–327.

560

561

562

563 **Figure Captions:**

564

565 **Figure 1: Distribution of a) meteoric water and b) permeability with depth.** Deuterium excess  
566 and  $^{18}\text{O}$  depletion generally decreases with depth showing a transition from waters with a  
567 meteoric origin (D excess between -10 and 30‰ or  $^{18}\text{O}$  depletion from -1.25 to 3.75‰, see  
568 inset for distribution along GMWL) to more negative values associated with paleo-evaporated  
569 seawater in sedimentary basins. Waters from several hundreds of m deep in the Canadian  
570 Shield tend to plot with more positive  $^{18}\text{O}$  depletion (apparent negative D excess) values.  
571 Isotopic data references are included in the methods. Global databases of permeability  
572 (Achtziger-Zupančič et al., 2017; Ingebritsen & Manning, 1999) show permeability generally  
573 decreases with depth. Numerical models of thermal springs indicate elevated permeability is  
574 present to depths of several km in orogenic belts (Forster & Smith, 1989). However, similar  
575 permeabilities exist in regional aquifers in sedimentary basins (Medina et al., 2011; Phillips,  
576 2019; Zhang et al., 2016) where non-meteoric waters are present.

577

578 **Figure 2:** Conceptual figure showing trade-off between topographic gradient and negative  
579 buoyancy from presence of dense brines in the Driving Force Ratio (DFR; Equation 6) controlling  
580 circulation depth of meteoric waters through a sedimentary basin and an underlying crystalline  
581 basement.  $h_o$  is hydraulic head at a given reference density,  $z_{max}$  is maximum circulation depth,  
582  $F_p$  is the force associated with topographic differences, and  $F_b$  is the force of negative buoyancy.

583

584 **Figure 3: Meteoric water circulation depth across North America.** Depth of circulation as  
585 estimated from deepest sample with D excess value within 20‰ of the GMWL in a 2 degree by  
586 2 degree grid. Squares with solid black outlines are produced waters, red outlines from  
587 estimates based on geothermometry from springs, and dashed outlines samples from mines or  
588 other projects in Precambrian rock. Isotopic data references are included in the methods.

589

590 **Figure 4: Prediction of circulating vs stagnant fluids based on topographic gradients.** D excess  
591 between -10 and 30‰ ( $^{18}\text{O}$  depletion from -1.25 to 3.75‰) values indicating meteoric waters  
592 mainly occur where topographic drop to depth ratios exceed 0.2, the theoretical critical value  
593 required for a brine with a density of  $1,200 \text{ kg/m}^3$  to be trapped by negative buoyancy.  
594 Negative D excess indicative of non-meteoric, paleo-evaporated seawater derived brines tend  
595 to plot at low topographic drop to depth ratios. Strongly positive  $^{18}\text{O}$  depletion (negative D  
596 excess) values found in shield environments tend to plot at topographic drop to depth ratios  
597 near the critical value for trapping by negative buoyancy.

Figure 1.

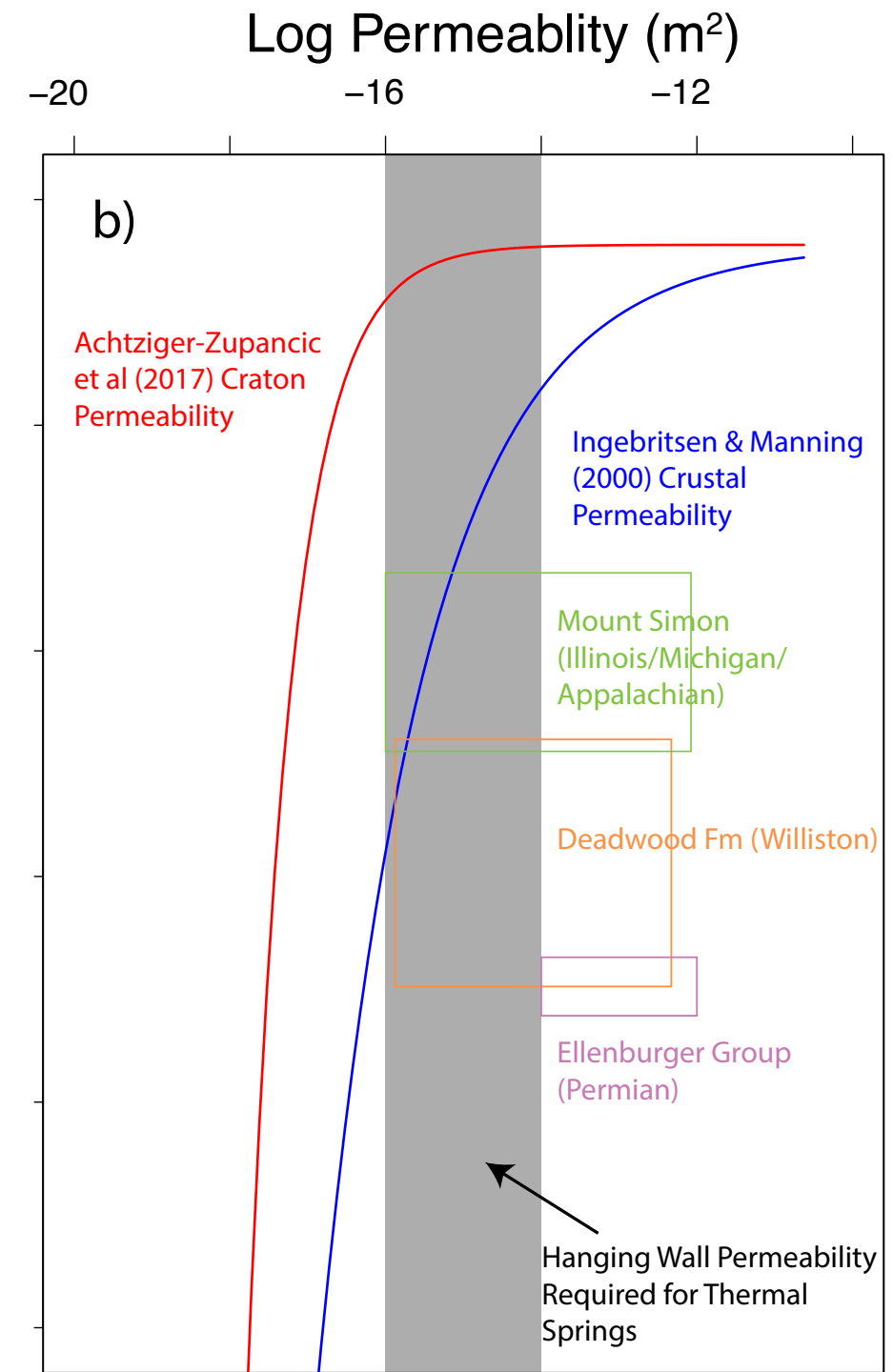
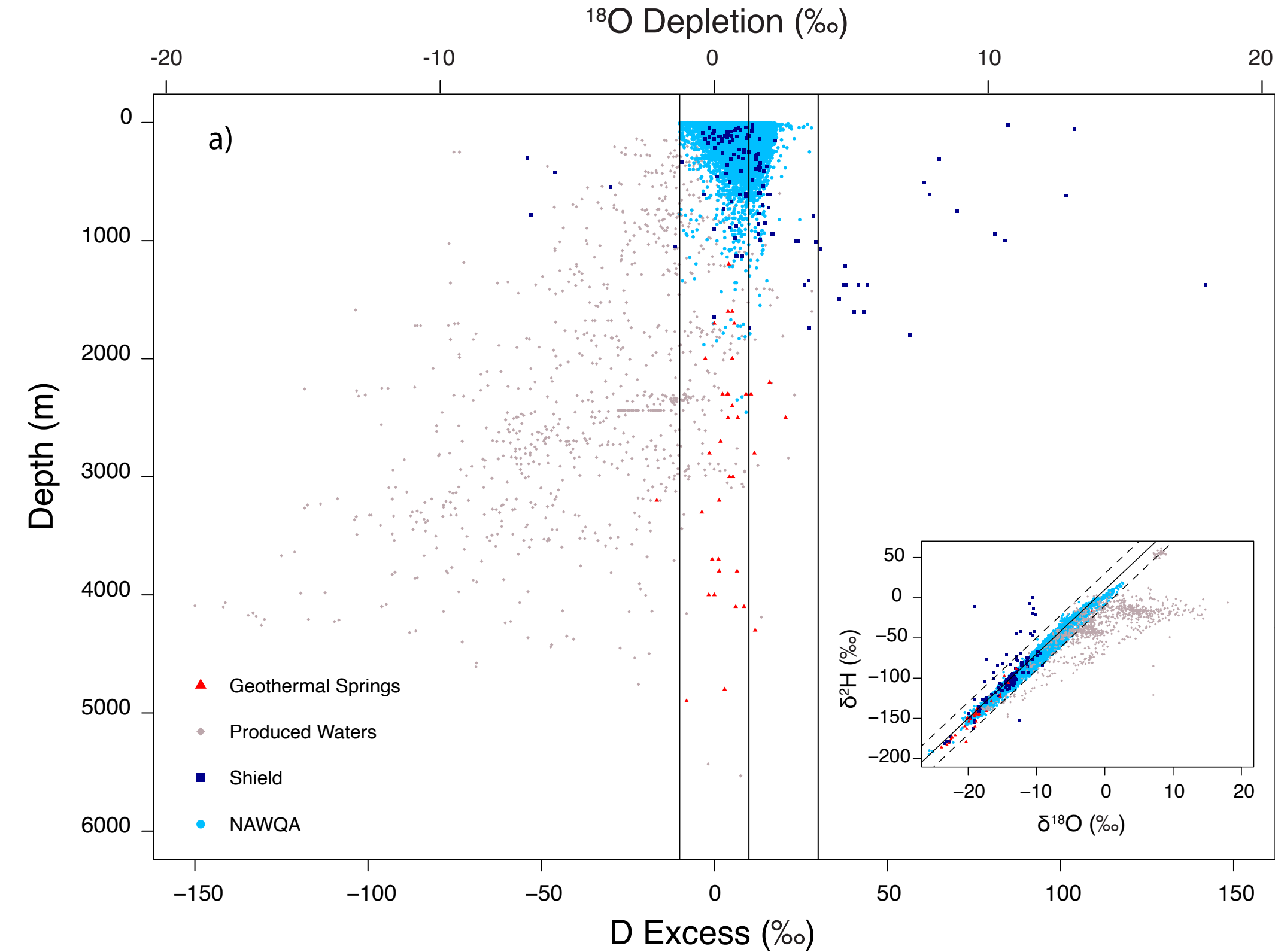


Figure 2.

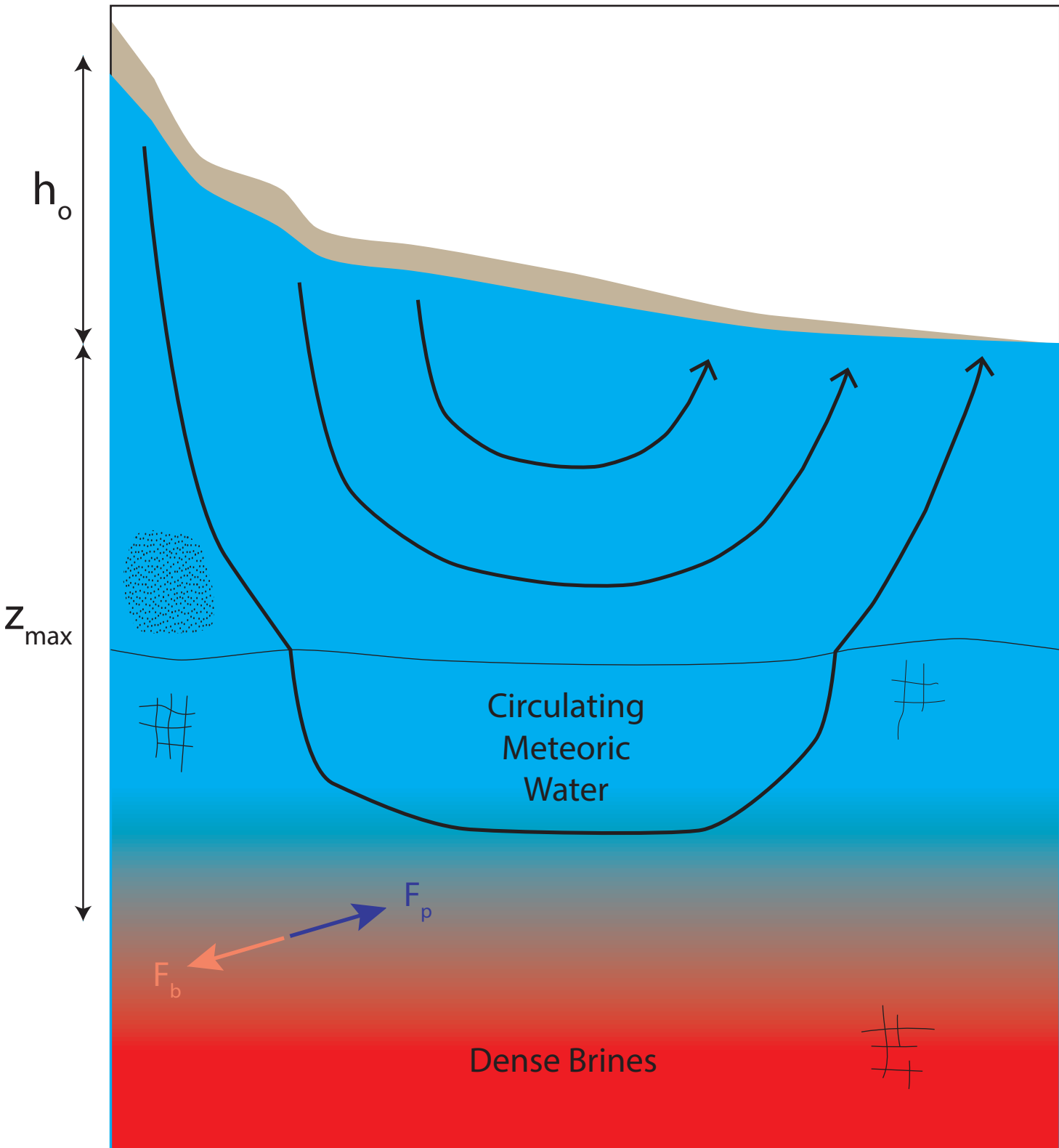
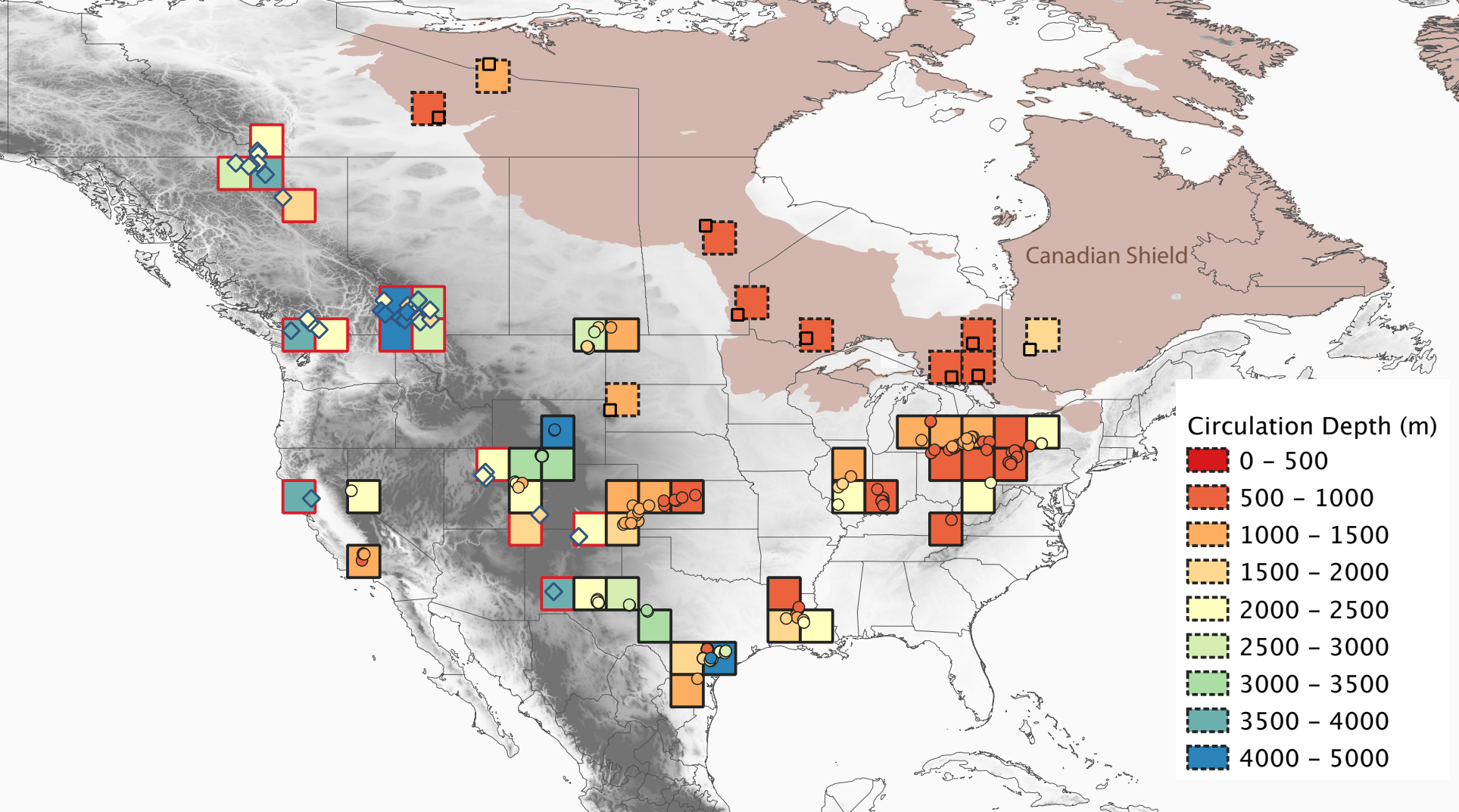


Figure 3.



**Figure 4.**

